



Coulomb electron pairing in a tight-binding model of La-based cuprate superconductors

Klaus M. Frahm and Dima L. Shepelyansky^a

Laboratoire de Physique Théorique, IRSAMC, Université de Toulouse, CNRS, UPS, 31062 Toulouse, France

Received 29 September 2020 / Accepted 11 November 2020

© EDP Sciences, SIF and Springer-Verlag GmbH Germany, part of Springer Nature 2020

Abstract. We study the properties of two electrons with Coulomb interactions in a tight-binding model of La-based cuprate superconductors. This tight-binding model is characterized by long-ranged hopping obtained previously by advanced quantum chemistry computations. We show analytically and numerically that the Coulomb repulsion leads to a formation of compact pairs propagating through the whole system. The mechanism of pair formation is related to the emergence of an effective narrow energy band for Coulomb electron pairs with conserved total pair energy and momentum. The dependence of the pair formation probability on an effective filling factor is obtained with a maximum around a filling factor of 20 (or 80) percent. The comparison with the case of the nearest neighbor tight-binding model shows that the long-ranged hopping provides an increase of the phase space volume with high pair formation probability. We conjecture that the Coulomb electron pairs discussed here may play a role in high temperature superconductivity.

1 Introduction

The phenomenon of high temperature superconductivity (HTC), discovered in [1], still requires its detailed physical understanding as discussed by various experts of this field (see e.g. [2–4]). The analysis is complicated by the complexity of the phase diagram and strong interactions between electrons (or holes). As a generic model, that can be used for a description of most superconducting cuprates, it was proposed to use a simplified one-body Hamiltonian with nearest-neighbor hopping on a square lattice formed by the Cu ions [5]. In addition the interactions between electrons are considered as a strongly screened Coulomb interaction that results in the 2D Hubbard model [5]. However, a variety of experimental results cannot be described by the 2D Hubbard model (see e.g. discussion in [6]). Other models of type Emery [7–10] were developed and extended on the basis of extensive computations with various numerical methods of quantum chemistry (see e.g. [6, 11] and Refs. therein). These studies demonstrated the importance of next-nearest hopping and allowed to determine reliably the longer-ranged tight-binding parameters.

In this work we use the 2D longer-ranged tight-binding parameters reported in [6] and study the effects of Coulomb interactions between electrons in the frame

work of this tight-binding model. There are different reasons indicating that long-range interactions between electrons may lead to certain new features as compared to the Hubbard case (see [3, 4, 6]). Recently, we demonstrated that for two electrons on a 2D lattice with nearest-neighbor hopping the energy and momentum conservation laws lead to the appearance of an effective narrow energy band for energy dispersion of two electrons [12]. In such a narrow band even a repulsive Coulomb interaction leads to electron pairing and ballistic propagation of such pairs through the whole system. The internal classical dynamics of electrons inside such a pair is chaotic suggesting nontrivial properties of pair formation in the quantum case. In this work we extend the investigations of the properties of such Coulomb electron pairs for a more generic longer-ranged tight-binding lattice of one-body Hamiltonian typical for La-based cuprate superconductors. We find that the long-ranged hopping leads to new features of Coulomb electron pairs. We note that in this work we consider the case of two interacting electrons but the same results are valid also for two interacting holes with positive charges.

In Sect. 2 a detailed description of the tight-binding model for two interacting electrons for general lattices with a particular application to HTC is presented together with an analysis of the effective band width at fixed conserved total pair momentum. Section 3 provides first results of the full space time evolution obtained in the frame work of the Trotter formula approximation. Section 4 introduces the theoretical basis for the description in terms of an effective

Supplementary information The online version of this article (<https://doi.org/10.1140/epjb/s10051-020-00035-1>) contains supplementary information, which is available to authorized users.

^ae-mail: dima@irsamc.ups-tlse.fr (corresponding author)

block Hamiltonian for a given sector of fixed momentum of a pair with technical details provided in Appendix A. In Sect. 5 the phase diagram of the long time average of the pair formation probability in the plane of total momentum is discussed while Sect. 6 provides some results for the intermediate time evolution of pair formation. An overview of the results for the pair formation probability at different filling factors is given in Sect. 7. The final discussion is presented in Sect. 8.

2 Generalized tight-binding model on a 2D lattice

We assume that each electron moves on a square lattice of size $N \times N$ with periodic boundary conditions with respect to the following generalized one-particle tight-binding Hamiltonian:

$$H_{1p} = - \sum_{\mathbf{r}} \sum_{\mathbf{a} \in \mathcal{A}} t_{\mathbf{a}} (|\mathbf{r}\rangle \langle \mathbf{r} + \mathbf{a}| + |\mathbf{r} + \mathbf{a}\rangle \langle \mathbf{r}|) \quad (1)$$

where the first sum is over all discrete lattice points \mathbf{r} (measured in units of the lattice constant) and \mathbf{a} belongs to a certain set of neighbor vectors \mathcal{A} such that for each lattice state $|\mathbf{r}\rangle$ there are non-vanishing hopping matrix elements $t_{\mathbf{a}}$ with $|\mathbf{r} + \mathbf{a}\rangle$ and $|\mathbf{r} - \mathbf{a}\rangle$ for $\mathbf{a} \in \mathcal{A}$. To be more precise, due to notational reasons, we choose the set \mathcal{A} to contain all neighbor vectors $\mathbf{a} = (a_x, a_y)$ in one half plane with either $a_x > 0$ or $a_y > 0$ if $a_x = 0$ such that $\mathcal{A}' = \mathcal{A} \cup (-\mathcal{A})$ is the full set of all neighbor vectors. For each vector \mathbf{a} of the full set \mathcal{A}' , we require that any other vector $\tilde{\mathbf{a}}$ which can be obtained from \mathbf{a} by a reflection at either the x -axis, y -axis or the x - y diagonal also belongs to the full set \mathcal{A}' and has the same hopping amplitude $t_{\mathbf{a}} = t_{\tilde{\mathbf{a}}}$.

For the usual nearest neighbor tight-binding model (NN-model), already considered in [12], we have the set $\mathcal{A}_{\text{NN}} = \{(1, 0), (0, 1)\}$ with $t_{(1,0)} = t_{(0,1)} = t = 1$. The numerical results presented in this work correspond either to the NN-model (for illustration and comparison) or to a longer-ranged tight-binding lattice according to [6] which we denote as the HTC-model. For this case the set of neighbor vectors is $\mathcal{A}_{\text{HTC}} = \{(1, 0), (0, 1), (2, 0), (0, 2), (1, \pm 2), (2, \pm 1), (1, \pm 1), (2, \pm 2)\}$ and the hopping amplitudes are: $t = t_{(1,0)} = 1$, $t' = t_{(1,1)} = -0.136$, $t'' = t_{(2,0)} = 0.068$, $t''' = t_{(2,1)} = 0.061$ and $t^{(4)} = t_{(2,2)} = -0.017$ corresponding to the values given in Table 2 of [6] (all energies are measured in units of the hopping amplitude $t = t_{(1,0)} = t_{(0,1)}$ which is therefore set to unity here; see also Fig. 6a of [6] for the neighbor vectors of the different hopping amplitudes). The hopping amplitudes for other vectors such as $(0, 1)$, $(1, -1)$, $(2, 1)$, $(1, -2)$ etc. are obtained from the above amplitudes by the appropriate symmetry transformations, e.g. $t_{(1,-1)} = t_{(1,1)} = t' = -0.136$ etc.

Even though that most of our numerical results presented in this work apply to the HTC-model (or

the NN-model), we emphasize that certain theoretical considerations given below, especially for the effective block Hamiltonian in relative coordinates at given total momentum, are valid for arbitrary generalized tight binding models with more general sets \mathcal{A} and also with a potential generalization to other dimensions.

The eigenstates of H_{1p} given in (1) are simple plane waves:

$$|\mathbf{p}\rangle = \frac{1}{N} \sum_{\mathbf{r}} e^{i\mathbf{p}\cdot\mathbf{r}} \quad (2)$$

with energy eigenvalues:

$$E_{1p}(\mathbf{p}) = -2 \sum_{\mathbf{a} \in \mathcal{A}} t_{\mathbf{a}} \cos(\mathbf{p} \cdot \mathbf{a}) \quad (3)$$

and momenta $\mathbf{p} = (p_x, p_y)$ such that p_x and p_y are integer multiples of $2\pi/N$ (i.e. $p_{\alpha} = 2\pi l_{\alpha}/N$, $l_{\alpha} = 0, \dots, N-1$, $\alpha = x, y$). For the HTC model, we can give a more explicit expression of the energy dispersion:

$$\begin{aligned} E_{1p}(p_x, p_y) = & -2 [\cos(p_x) + \cos(p_y)] \\ & - 4t' \cos(p_x) \cos(p_y) \\ & - 2t'' [\cos(2p_x) + \cos(2p_y)] \\ & - 4t''' [\cos(2p_x) \cos(p_y) + \cos(2p_y) \cos(p_x)] \\ & - 4t^{(4)} \cos(2p_x) \cos(2p_y) \end{aligned} \quad (4)$$

which corresponds to eq. (30) of [6] (assuming $t = 1$ and $t^{(5)} = t^{(6)} = t^{(7)} = 0$).

The quantum Hamiltonian of the model with two interacting particles (TIP) has the form:

$$H = H_{1p}^{(1)} \otimes \mathbf{1}^{(2)} + \mathbf{1}^{(1)} \otimes H_{1p}^{(2)} + \sum_{\mathbf{r}_1, \mathbf{r}_2} \bar{U}(\mathbf{r}_2 - \mathbf{r}_1) |\mathbf{r}_1, \mathbf{r}_2\rangle \langle \mathbf{r}_1, \mathbf{r}_2| \quad (5)$$

where $H_{1p}^{(j)}$ is the one-particle Hamiltonian (1) of particle $j = 1, 2$ with positional coordinate $\mathbf{r}_j = (x_j, y_j)$ and $\mathbf{1}^{(j)}$ is the unit operator of particle j . The last term in (5) represents a (regularized) Coulomb type long-range interaction $\bar{U}(\mathbf{r}_2 - \mathbf{r}_1) = U/[1 + r(\mathbf{r}_2 - \mathbf{r}_1)]$ with amplitude U and the effective distance $r(\mathbf{r}_2 - \mathbf{r}_1) = \sqrt{\Delta\bar{x}^2 + \Delta\bar{y}^2}$ between the two electrons on the lattice with periodic boundary conditions. (Here $\Delta\bar{x} = \min(\Delta x, N - \Delta x)$; $\Delta\bar{y} = \min(\Delta y, N - \Delta y)$; $\Delta x = x_2 - x_1$; $\Delta y = y_2 - y_1$ and the latter differences are taken modulo N , i.e. $\Delta x = N + x_2 - x_1$ if $x_2 - x_1 < 0$ and similarly for Δy). Furthermore, we consider symmetric (spatial) wavefunctions with respect to particle exchange assuming an antisymmetric spin-singlet state (similar results are obtained for antisymmetric wavefunctions).

In absence of interaction ($U = 0$) the energy eigenvalues (the classical energy) of the two electron Hamiltonian (5) (the two electrons) at given momenta \mathbf{p}_1 and

\mathbf{p}_2 are (is) given by:

$$\begin{aligned} E_c(\mathbf{p}_1, \mathbf{p}_2) &= E_{1p}(\mathbf{p}_1) + E_{1p}(\mathbf{p}_2) \\ &= -4 \sum_{\mathbf{a} \in \mathcal{A}} t_{\mathbf{a}} \cos(\mathbf{p}_+ \cdot \mathbf{a}/2) \cos(\Delta\mathbf{p} \cdot \mathbf{a}) \quad (6) \end{aligned}$$

where $\mathbf{p}_+ = \mathbf{p}_1 + \mathbf{p}_2$ is the total momentum and $\Delta\mathbf{p} = (\mathbf{p}_2 - \mathbf{p}_1)/2$ is the momentum associated to the relative coordinate $\Delta\mathbf{r} = \mathbf{r}_2 - \mathbf{r}_1$. For the NN-model Eq. (6) becomes $E_c(\mathbf{p}_1, \mathbf{p}_2) = -4 \sum_{\alpha=x,y} \cos(p_{+\alpha}/2) \cos(\Delta p_{\alpha})$.

Due to the translational invariance the total momentum \mathbf{p}_+ is conserved even in the presence of interaction ($U \neq 0$). Indeed, like in a periodic crystal we have Bloch waves with conserved quasimomentum [6] (in the following we speak about the momentum). Thus only two-particle plane wave states with identical \mathbf{p}_+ are coupled by non-vanishing interaction matrix elements. For the case of the NN-model, analyzed in [12], the kinetic energy at fixed \mathbf{p}_+ is bounded by $\Delta E_b = 4 \sum_{\alpha=x,y} |\cos(p_{+\alpha}/2)|$. Thus for TIP states with $E > \Delta E_b$ the two electrons cannot separate and propagate as one pair even if their interaction is repulsive. For $p_{+x} = p_{+y} = \pi + \delta$ being close to π and $|\delta| \ll 1$ there are compact Coulomb electron pairs even for very small interactions U as soon as $\Delta E_b \approx 4|\delta| < U \ll B_2$ with $B_2 = 16 + U$ being the maximal energy bandwidth¹ in 2D. Thus the conservation of the total momentum of a pair with $p_{+x} = p_{+y} \approx \pi$ leads to the appearance of an effective narrow energy band with formation of coupled electron pairs propagating through the whole system. However, the results obtained in [12] show that even for other values of p_{+x}, p_{+y} the probability of pair formation is rather high.

For the NN-model the effective band width for pairs ΔE_b can be exactly zero for the specific pair momentum $\mathbf{p}_+ = (\pi, \pi)$. However, this is not the case for the HTC-model where due to the longer-ranged hopping the minimal width ΔE_b is finite due to the additional terms with factors $\cos(\mathbf{p}_+ \cdot \mathbf{a}/2)$ in (6). Therefore, we determined numerically for each given value of total momentum \mathbf{p}_+ the effective bandwidth as:

$$\Delta E_b(\mathbf{p}_+) = \max_{\Delta\mathbf{p}} [E_c(\mathbf{p}_1, \mathbf{p}_2)] - \min_{\Delta\mathbf{p}} [E_c(\mathbf{p}_1, \mathbf{p}_2)] \quad (7)$$

with $\mathbf{p}_1 = \mathbf{p}_+/2 - \Delta\mathbf{p}$ and $\mathbf{p}_2 = \mathbf{p}_+/2 + \Delta\mathbf{p}$. Top panels of Fig. 1 show density color plots of $\Delta E_b(\mathbf{p}_+)$ for the NN- and the HTC-model. For the HTC-case $\Delta E_b(\mathbf{p}_+)$ is maximal at $\mathbf{p}_+ = (0, 0)$ with value $\Delta E_{b,\max} = 17.952$ and minimal at $\mathbf{p}_+ = (\pi, \pi)$ with value $\Delta E_{b,\min} = 2.176$ while for the NN-model we have $\Delta E_{b,\max} = 16$ at $\mathbf{p}_+ = (0, 0)$ and $\Delta E_{b,\min} = 0$ at $\mathbf{p}_+ = (\pi, \pi)$. The value $\Delta E_{b,\min} = 2.176$ for the HTC-model is still rather small compared to the maximal value $\Delta E_{b,\max} \approx 18$ and we may expect a somewhat stronger pair formation probability for total momenta \mathbf{p}_+ close to (π, π) . However, this situation is qualitatively different as compared to

¹ In the following we use the notation $B_2 = 16 + U$ for the bandwidth of the NN-model.

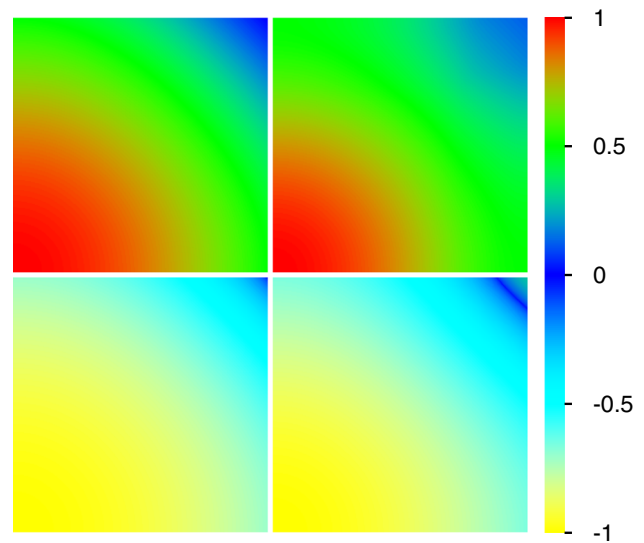


Fig. 1 Top panels show the dependence of the effective electron pair band width $\Delta E_b(\mathbf{p}_+)$ on the pair momentum $\mathbf{p}_+ = (p_{+x}, p_{+y})$. Bottom panels show the kinetic electron pair energy $E_c(\mathbf{p}_1, \mathbf{p}_2)$ (in absence of interaction) at momenta $\mathbf{p}_1 = \mathbf{p}_2 = \mathbf{p}_+/2$. Left panels correspond to the NN-model and right panels to the HTC-model. In all panels the horizontal axis corresponds to $p_{+x} \in [0, \pi]$ and the vertical axis to $p_{+y} \in [0, \pi]$. The numbers of the color bar correspond for top panels to the ratio of the bandwidth over its maximal value and for lower panels to the quantity $\text{sgn}(E_c) \sqrt{|E_c|/E_{c,\max}}$ with $E_{c,\max}$ being the maximum of $|E_c|$. In all subsequent color plot figures the numerical values of the color bar corresponds to the ratio of the shown quantity over its maximal value

the NN-model and the HTC-case requires new careful studies.

For comparison, we also show in the lower panels of Fig. 1 the kinetic energy E_c at $\mathbf{p}_1 = \mathbf{p}_2 = \mathbf{p}_+/2$ (for the square $\mathbf{p}_+ \in [0, \pi] \times [0, \pi]$) corresponding to $\Delta\mathbf{p} = 0$. While for the NN-model this quantity vanishes at $\mathbf{p}_+ = (\pi, \pi)$ there is for the HTC-model a zero-line between the two points $(\beta\pi, \pi)$ and $(\pi, \beta\pi)$ where $\beta \approx 0.877 \approx 7/8$ is a numerical constant slightly below unity.

3 Full space time evolution of electron pairs

As in [12] the full time evolution of two electrons is computed numerically for $N = 128$ using the Trotter formula approximation (see e.g. [12, 13] for computational details). We use the Trotter time step $\Delta t = B_2 = 1/(16 + U)$ which is the inverse bandwidth for the case of NN-model. A further decrease of the time step does not affect the obtained results. At the initial time both electrons are localized approximately at $(N/2, N/2)$ with the distance $\Delta x = \Delta y = 1$ using a linear combination of 8 states with all combinations due to particle exchange symmetry and reflection symmetry at the Δx - and Δy -axis. The method provides for each

223 time value a wavefunction $\psi(x_1, y_1, x_2, y_2)$ from which
 224 we extract different quantities such as the density in
 225 x_1 - x_2 plane:

$$226 \quad \rho_{XX}(x_1, x_2) = \sum_{y_1, y_2} |\psi(x_1, y_1, x_2, y_2)|^2 \quad (8)$$

227 or the density Δx - Δy plane:

$$228 \quad \rho_{\text{rel}}(\Delta x, \Delta y) = \sum_{x_1, y_1} |\psi(x_1, y_1, x_1 + \Delta x, y_1 + \Delta y)|^2 \quad (9)$$

229 (with position sums taken modulo N). We also compute
 230 the quantity w_{10} by summing the latter density (9) over
 231 all values such that $|\Delta \bar{x}| \leq 10$ and $|\Delta \bar{y}| \leq 10$ which
 232 corresponds to a square of size 21×21 in Δx - Δy plane
 233 (due to negative values of $x_2 - x_1$ etc.). This quantity
 234 gives the quantum probability to find both electrons at
 235 a distance ≤ 10 (in each direction) and we will refer to
 236 it as the *pair formation probability*.

237 In Fig. 2 the density ρ_{XX} is shown for $U = 2$, both
 238 NN- and HTC-models at two time values $t = 445\Delta t$
 239 and $t = 10^4 \Delta t$. These results show that the wavefunc-
 240 tion has a component with electrons separating from
 241 each other and a component where electrons stay close
 242 to each other forming a pair propagating through the
 243 whole system that corresponds to a high density near
 244 a diagonal with $x_1 \approx x_2$. For $t = 445\Delta t$ the value of
 245 w_{10} is roughly 10% and for $t = 10^4 \Delta t$ it is roughly
 246 13% for both models. However, the remaining diffusing
 247 component of about 87-90% probability has a stronger
 248 periodic structure for the NN-model as compared to the
 249 HTC-model.

250 Figure 3 shows the density $\rho_{\text{rel}}(\Delta x, \Delta y)$ for the same
 251 cases of Fig. 2. We clearly see a strong enhancement of
 252 the probability at small values $\Delta \bar{x} \approx \Delta \bar{y} < 5$ ($< 6 - 7$)
 253 for the NN-model (HTC-model) showing that there is a
 254 considerable probability that both electrons stay close
 255 to each other forming a Coulomb electron pair. Fur-
 256 thermore, the remaining wavefunction component of
 257 independently propagating electrons, clearly visible in
 258 Fig. 2, is not visible in the density shown in Fig. 3 even
 259 though this component corresponds to 87-90% proba-
 260 bility.

261 The supplementary material contains two videos (for
 262 ~ 460 time values in the range $\Delta t \leq t \leq 10^4 \Delta t$ with
 263 roughly uniform logarithmic density) of the two den-
 264 sities ρ_{XX} and ρ_{rel} where both models NN and HTC
 265 are directly compared in the same video. The raw-data
 266 used for these videos is the same as in Figs. 2 and 3.

267 4 Time evolution in sectors of fixed total 268 momentum

269 As already mentioned in Sect. 3 the total momentum
 270 \mathbf{p}_+ is conserved by the TIP dynamics of the Hamil-
 271 tonian (5). In order to exploit this more explicitly, we

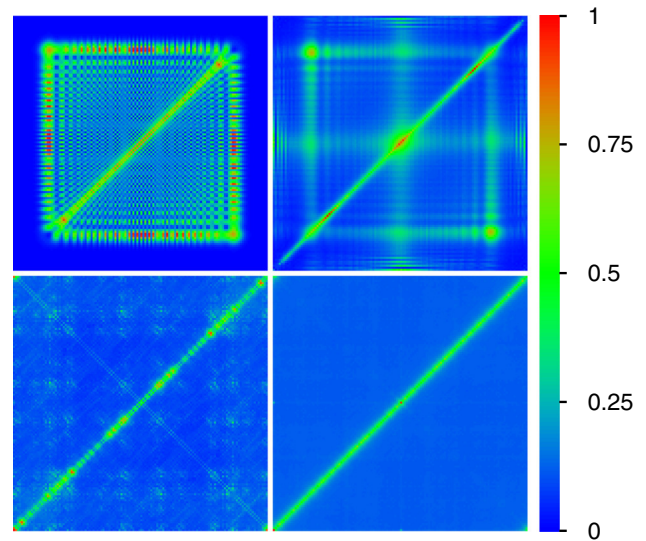


Fig. 2 2D Wavefunction density $\rho_{XX}(x_1, x_2)$ in x_1 - x_2 plane (see Eq. (8)) obtained from the time evolution using the Trotter formula approximation for initial electron positions at $\approx (N/2, N/2)$ with distance $\Delta \bar{x} = \Delta \bar{y} = 1$ for $N = 128$, $U = 2$ and Trotter integration time step $\Delta t = 1/B_2 = 1/(16 + U)$. Top (bottom) panels correspond to the time value $t = 445 \Delta t$ ($t = 10^4 \Delta t$) and left (right) panels correspond to the NN-lattice (HTC-lattice). The corresponding values of the pair formation probability w_{10} are 0.106 (top left), 0.133 (bottom left), 0.0940 (top right) and 0.125 (bottom right). Related videos are available at [14, 15]

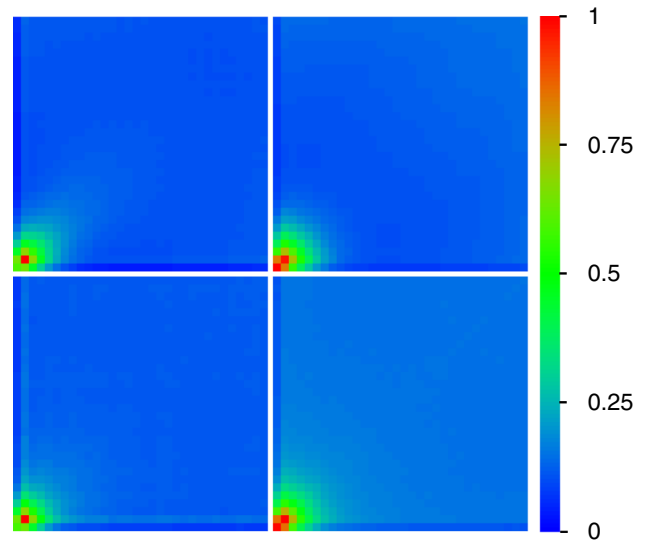


Fig. 3 2D Wavefunction density $\rho_{\text{rel}}(\Delta x, \Delta y)$ in Δx - Δy plane of relative coordinates (see Eq. (9)) for the same states, cases and parameters of Fig. 2 ($N = 128$, $U = 2$). All panels show the zoomed density for $0 \leq \Delta x, \Delta y < 32$. Related videos are available at [14, 15]

introduce as in [12], *block basis states* by:

$$|\mathbf{p}_+, \Delta \mathbf{r}\rangle = \frac{1}{N} \sum_{\mathbf{r}_1} e^{i\mathbf{p}_+ \cdot (\mathbf{r}_1 + \Delta \mathbf{r}/2)} |\mathbf{r}_1, \mathbf{r}_1 + \Delta \mathbf{r}\rangle \quad (10)$$

where $\mathbf{p}_+ = (p_{+x}, p_{+y})$ (with $p_{+\alpha} = 2\pi l_{+\alpha}/N$; $l_{+\alpha} = 0, \dots, N-1$; $\alpha = x, y$) is a fixed value of the total momentum and $\mathbf{r}_1, \Delta\mathbf{r}$ are vectors on the square lattice (with position sums in each spatial direction taken modulo N). One can show (see Appendix A for details) that the TIP Hamiltonian (5) applied to such state gives a linear combination of such states for different $\Delta\mathbf{r}$ values but the **same** total momentum value \mathbf{p}_+ which provides for each value or *sector* of \mathbf{p}_+ an effective *block Hamiltonian*:

$$\begin{aligned} \bar{h}^{(\mathbf{p}_+)} = & - \sum_{\Delta\mathbf{r}} \sum_{\mathbf{a} \in \mathcal{A}} \bar{t}_{\mathbf{a}}^{(\mathbf{p}_+)} (|\Delta\mathbf{r} + \mathbf{a}\rangle \langle \Delta\mathbf{r}| + |\Delta\mathbf{r}\rangle \langle \Delta\mathbf{r} + \mathbf{a}|) \\ & + \sum_{\Delta\mathbf{r}} \bar{U}(\Delta\mathbf{r}) |\Delta\mathbf{r}\rangle \langle \Delta\mathbf{r}| \end{aligned} \quad (11)$$

where $\bar{t}_{\mathbf{a}}^{(\mathbf{p}_+)} = 2 \cos(\mathbf{p}_+ \cdot \mathbf{a}/2) t_{\mathbf{a}}$ is an *effective rescaled hopping amplitude* depending also on \mathbf{p}_+ and we have for simplicity omitted the index \mathbf{p}_+ in the block basis states. This effective block Hamiltonian corresponds to a tight-binding model in 2D of similar structure as (1) with modified hopping amplitudes and an additional “potential” $\bar{U}(\Delta\mathbf{r})$. We note that in absence of this external potential ($U = 0$) the eigenfunctions of (11) are plane waves and we immediately recover the expression (6) for its energy eigenvalues where $\Delta\mathbf{p}$ is the momentum associated to the relative coordinate $\Delta\mathbf{r}$. For the simple NN-model the result for the effective block Hamiltonian was already given in [12] and the above expression (11) provides the generalization to arbitrary tight-binding lattices characterized by a certain set of neighbor vectors \mathcal{A} and associated hopping amplitudes $t_{\mathbf{a}}$ (the generalization to arbitrary spatial dimension is also obvious). As already discussed in [12] the boundary conditions of (11) in x - (y -)direction are either periodic if the integer index l_{+x} (l_{+y}) of p_{+x} (p_{+y}) is even or anti-periodic if this index is odd. This can be understood by the fact that the expression (10) is modified by the factor $e^{\pm i p_{+x} N/2} = e^{\pm i \pi l_{+x}} = (-1)^{l_{+x}}$ if Δx is replaced by $\Delta x \pm N$ and similarly for Δy (with $\Delta\mathbf{r} = (\Delta x, \Delta y)$).

Diagonalizing the effective block Hamiltonian (11), we can rather efficiently compute the exact quantum time evolution $|\bar{\psi}(t)\rangle = e^{-i\bar{h}^{(\mathbf{p}_+)} t} |\bar{\psi}(0)\rangle$ inside a given sector of \mathbf{p}_+ . As initial state $|\bar{\psi}(0)\rangle$ we choose a state (in the reduced block space) given as the totally symmetric superposition of four localized states where Δx and Δy are either 1 or $N-1$. Such a state corresponds in full space to a plane wave in the center of mass direction with total fixed momentum \mathbf{p}_+ and strongly localized in the relative coordinate $\Delta\mathbf{r}$. The matrix size of (11) is N^2 which corresponds to a complexity of N^6 for the numerical diagonalization.

However, for a general lattice, such as the HTC-model, one can exploit the particle exchange symmetry to reduce the effective matrix size to roughly $N^2/2$ and for the special cases of $p_{+x} = p_{+y}$ or either $p_{+x} = 0$ or $p_{+y} = 0$ a second symmetry allows a further reduction of the effective matrix size to $\approx N^2/4$ (for the

NN-model there are two or three symmetries for these cases with effective matrix sizes of $\approx N^2/4$ or $\approx N^2/8$ respectively; see [12] and Appendix A for details).

In view of this, we have been able to compute numerically the exact time evolution for the HTC-model in certain \mathbf{p}_+ sectors for a lattice size up to $N = 384$ for the case of two symmetries and a limited number of different other parameters (values of \mathbf{p}_+ and U). For the case of one symmetry and the exploration of all possible values of p_{+x} and p_{+y} we used the maximum system size $N = 192$. We also implemented more expensive computations where no or less possible symmetries are used to verify (at smaller values of N) that they provide identical numerical results.

We compute the wavefunction in block representation $\bar{\psi}(\mathbf{p}_+, \Delta\mathbf{r})$ for about 700 time values $t = 0$ and $10^{-1} \leq t/\Delta t \leq 10^6$ (with a uniform density in logarithmic scale) where $\Delta t = 1/B_2 = 1/(16 + U)$ is the time step already used for the Trotter formula approximation given as the inverse bandwidth for the case of the NN-model which is the smallest time (inverse of the largest energy) scale of the system.

From the wavefunction we extract in a similar way as in Sect. 3 the pair formation probability w_{10} by summing the (normalized) wavefunction density $|\bar{\psi}(\mathbf{p}_+, \Delta\mathbf{r})|^2$ at fixed \mathbf{p}_+ over the 21×21 square with $|\Delta\bar{x}| \leq 10$ and $|\Delta\bar{y}| \leq 10$. We also compute the inverse participation ratio:

$$\xi_{\text{IPR}} = \left(\sum_{\Delta\mathbf{r}} |\bar{\psi}(\mathbf{p}_+, \Delta\mathbf{r})|^4 \right)^{-1} \quad (12)$$

which gives roughly the number of lattice sites (in $\Delta\mathbf{r}$ space) over which the wavefunction is localized. Both quantities w_{10} and ξ_{IPR} converge typically rather well to their stationary values at times $t > 10^3 \Delta t$ with some time dependent fluctuations. Therefore for the cases where we are interested in the long time limit we compute the wavefunction only for 70 times values (in the same interval as above with uniform logarithmic density) and take the average over the 21 values with $10^4 \leq t/\Delta t \leq 10^6$. We note that for the case of a uniform wavefunction density the *ergodic* values are $w_{10, \text{erg}} = (21/N)^2$ and $\xi_{\text{IPR, erg}} = N^2$. Values of w_{10} significantly above $w_{10, \text{erg}}$ or of ξ_{IPR} below $\xi_{\text{IPR, erg}}$ indicate an enhanced probability for the formation of compact electron pairs.

We also mention that both quantities w_{10} and ξ_{IPR} are invariant with respect to the three transformations $p_{+x} \leftrightarrow p_{+y}$, $p_{+x} \rightarrow -p_{+x}$ and $p_{+y} \rightarrow -p_{+y}$ (or $p_{+x} \rightarrow 2\pi - p_{+x}$ and $p_{+y} \rightarrow 2\pi - p_{+y}$) corresponding to reflections at the x - y diagonal, the y -axis and the x -axis. Even though the effective block Hamiltonian (11) is not (always) invariant with respect to all three of these transformations (see Appendix A for details), the choice of an invariant initial state ensures that at finite times the wavefunction in block space satisfies for example the identity $\bar{\psi}(p_{+x}, p_{+y}, \Delta x, \Delta y) = \bar{\psi}(p_{+y}, p_{+x}, \Delta y, \Delta x)$ (and similarly for the other reflec-

384 tions). In other words a certain reflection transformation
 385 for \mathbf{p}_+ results in the equivalent transformation for
 386 the time dependent block space wavefunction in $\Delta\mathbf{r}$
 387 space. Obviously the two quantities w_{10} and ξ_{IPR} do
 388 not change with respect to these transformations (in
 389 $\Delta\mathbf{r}$ space) and therefore they are conserved. As a result
 390 it is sufficient to compute these quantities only for the
 391 triangle $0 \leq p_{+y} \leq p_{+x} \leq \pi$.

392 In the following sections we present the results for
 393 these quantities and the wavefunction in block representation.
 394

395 5 Phase diagram of pair formation

396 The phase diagram of the long time average of the pair
 397 formation probability w_{10} in the \mathbf{p}_+ -plane is shown
 398 in Fig. 4 for both models and the interaction values
 399 $U = 0.5, 2$. As expected from the features of the effective
 400 bandwidth shown in (the top panels of) Fig. 1, we
 401 find that globally for both models the pair formation
 402 probability is clearly maximal at $\mathbf{p}_+ = (\pi, \pi)$ and minimal
 403 at $\mathbf{p}_+ = (0, 0)$. Furthermore, the size of the maxi-

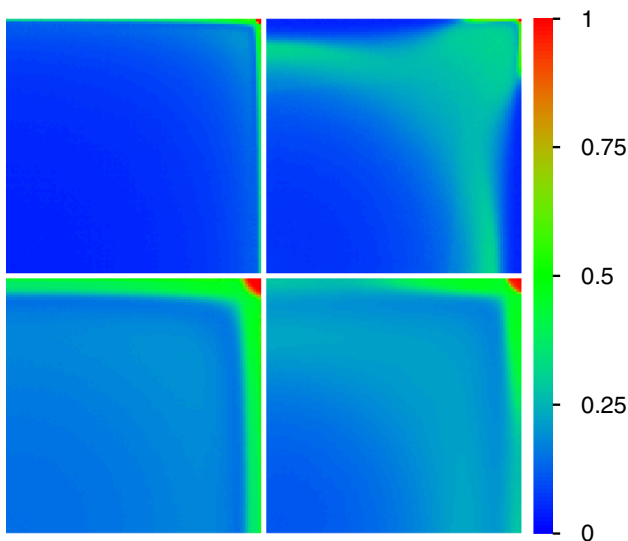


Fig. 4 Phase diagram of electron pair formation in the plane of pair momentum $\mathbf{p}_+ = (p_{+x}, p_{+y})$ for the NN-lattice (left panels), the HTC-lattice (right panels) and the interaction values $U = 0.5$ (top panels), $U = 2$ (bottom panels). Shown is the pair formation probability w_{10} for $N = 192$ obtained from the exact time evolution for each sector of \mathbf{p}_+ with an initial electron distance $\Delta\bar{x} = \Delta\bar{y} = 1$ and computed from an average over 21 time values in the interval $10^4 \leq t/\Delta t \leq 10^6$. In all panels the horizontal (vertical) axis corresponds to p_{+x} (p_{+y}) $\in [0, \pi]$ and the numerical values of the color bar correspond to the ratio of w_{10} over its maximal value. The maximum values corresponding to the red region at the top right corner $\mathbf{p}_+ = (\pi, \pi)$ are $w_{10} = 1$ (both left panels), $w_{10} = 0.4510$ (top right) and $w_{10} = 0.8542$ (bottom right). For comparison the ergodic value is $w_{10, \text{erg.}} = (21/192)^2 = 0.01196$

404 mum region is significantly stronger for $U = 2$ than for
 405 $U = 0.5$ which is also to be expected. Thus for these
 406 \mathbf{p}_+ values even a relatively weak or moderate Coulomb
 407 repulsion creates quite strongly coupled electron pairs.

408 For the NN-model the top ($p_{+y} = \pi$) or right ($p_{+x} =$
 409 π) boundary also provide large values with $w_{10} \approx 0.5$
 410 and the width of these regions is stronger for $U = 2$
 411 than for $U = 0.5$. However, for $U = 2$ also the remain-
 412 ing region provides values between 0.14 and 0.25 of the
 413 maximum value which are clearly above the ergodic
 414 value 0.012. Even for $U = 0.5$ the remaining region
 415 is mostly ≈ 0.04 (with some part close to 0.25) which
 416 is still above the ergodic value.

417 For the HTC-model the situation is more compli-
 418 cated. The boundary regions are more limited, espe-
 419 cially for $U = 0.5$. However, for the remaining region
 420 there is a new interesting feature which is a signifi-
 421 cantly enhanced “green-circle” of approximate radius

$$r_g = \sqrt{p_{+x}^2 + p_{+y}^2} \approx 0.85\pi \text{ for } U = 0.5 \text{ (} w_{10} \approx 0.14\text{)}.$$

422 For $U = 2$ there is also a circle ($w_{10} \approx 0.20$) with
 423 approximate radius $r_g \approx 0.75\pi$. This circle seems to be
 424 less pronounced despite its larger value of w_{10} as com-
 425 pared to $U = 0.5$ due to the fact that the maximum
 426 value for $U = 2$ ($w_{10} \approx 0.85$ at $\mathbf{p}_+ = (\pi, \pi)$) is roughly
 427 twice the maximum value for $U = 0.5$ ($w_{10} \approx 0.45$).
 428 This structure cannot be explained by the behavior of
 429 the effective bandwidth. The minimum values of w_{10} at
 430 $\mathbf{p}_+ \approx (0, 0)$ are $w_{10} \approx 0.02 - 0.03$ ($w_{10} \approx 0.09 - 0.10$)
 431 for $U = 0.5$ ($U = 2$) which are slightly (significantly)
 432 above the ergodic value 0.012.

433 Globally, nearly for all values of \mathbf{p}_+ , for both mod-
 434 els and both interaction values $U = 0.5, 2$ there is an
 435 enhanced probability to create coupled electron pairs.
 436

437 The above observations are perfectly confirmed by
 438 the phase diagram for the inverse participation ratio
 439 ξ_{IPR} which is shown in Fig. 5 for the same cases and raw
 440 data of Fig. 4. Large (small) values of ξ_{IPR} corresponds
 441 to small (large) values of w_{10} and a small (strong) pair
 442 formation probability. Here minimum (maximum) val-
 443 ues are at $\mathbf{p}_+ = (\pi, \pi)$ ($\mathbf{p}_+ = (0, 0)$) as for the effective
 444 bandwidth of Fig. 1 (see figure caption for the numerical
 445 minimum, maximum and ergodic values). The bound-
 446 ary structure of the NN-model and the circle-structure
 447 of the HTC-case are also clearly visible.

448 We have also computed the long time average of the
 449 pair formation probability for the HTC-model at larger
 450 system size $N = 256$ and the special cases of either
 451 $p_{+x} = p_{+y}$ or $p_{+y} = 0$ where the additional second
 452 symmetry (see discussion in the previous section and
 453 Appendix A) reduces the computational effort. In this
 454 way we can explore the diagonal and right boundary of
 455 the phase diagram in more detail.

456 Figure 6 shows w_{10} for the HTC-model, $N = 256$,
 457 $p_+ = p_{+x} = p_{+y}$ and both interaction values $U = 0.5, 2$
 458 as a function of the parameter $\nu = (1 - \cos(p_+/2))/2$.
 459 Both curves clearly confirm some of the observations of
 460 the phase diagrams, i.e. strongest pair formation prob-
 461 ability at $\nu = 0.5$ ($p_{+x,y} = \pi$) with a somewhat larger
 462 maximum range for $U = 2$ as compared to $U = 0.5$
 463 and a minimal pair formation probability at $\nu = 0$

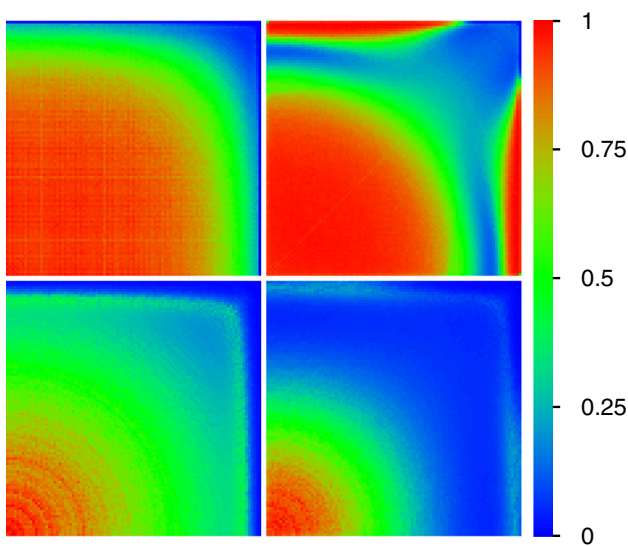


Fig. 5 Phase diagram of the inverse participation ratio ξ_{IPR} in the plane of pair momentum $\mathbf{p}_+ = (p_{+x}, p_{+y})$ and computed from the same states, data and cases as in Fig. 4 ($U = 0.5, 2$ in top/bottom panels; $N = 192$). The maximum values corresponding to the red region close to the bottom left corner $\mathbf{p}_+ = (0, 0)$ are $\xi_{IPR} = 15300$ (top left), $\xi_{IPR} = 4300$ (bottom left), $\xi_{IPR} = 18200$ (top right) and $\xi_{IPR} = 8600$ (bottom right). The minimum values at the top right corner $\mathbf{p}_+ = (\pi, \pi)$ are $\xi_{IPR} = 14.87$ (top left), $\xi_{IPR} = 4$ (bottom left), $\xi_{IPR} = 126$ (top right) and $\xi_{IPR} = 9.8$ (bottom right). For comparison the ergodic value is $\xi_{IPR,erg} = 192^2 = 36864$ and the value for the totally symmetrized and localized initial state is $\xi_{IPR,init} = 4$

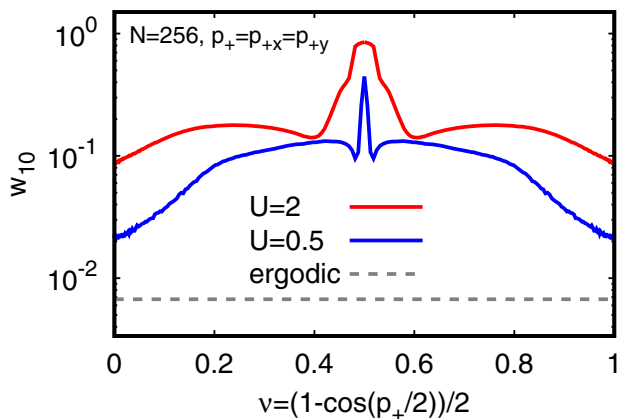


Fig. 6 Dependence of the electron pair formation probability w_{10} on $\nu = (1 - \cos(p_+/2))/2$ for $p_+ = p_{+x} = p_{+y}$ and the HTC-model at $U = 0.5, 2$ and $N = 256$. w_{10} is computed from the same long time average as in Fig. 4. The maximum value at $\nu = \nu_{max} = 0.5$ is $w_{10} = 0.8535$ ($w_{10} = 0.4456$) for $U = 2$ ($U = 0.5$). See Fig. 5 of [12] for the corresponding figure for the NN-model. For the NN-model the maximum value at $\nu = \nu_{max} = 0.5$ is exactly $w_{10} = 1$ for both interaction values

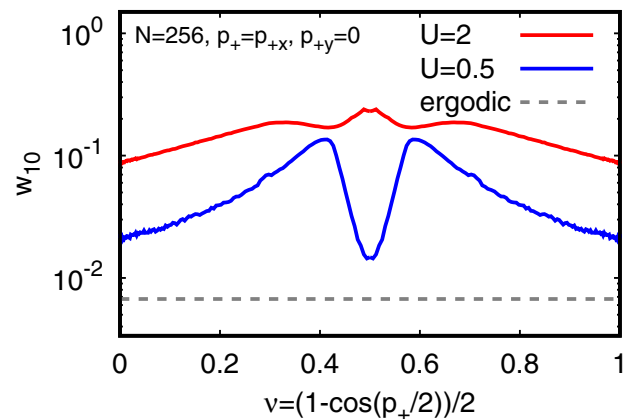


Fig. 7 Dependence of the electron pair formation probability w_{10} on $\nu = (1 - \cos(p_+/2))/2$ for $p_+ = p_{+x}, p_{+y} = 0$ and the HTC-model at $U = 0.5, 2$ and $N = 256$. w_{10} is computed from the same long time average as in Fig. 4. The value at $\nu = 0.5$ is $w_{10} = 0.2302$ ($w_{10} = 0.01479$) for $U = 2$ ($U = 0.5$)

ical maximum values of w_{10} at $\nu = 0.5$ are slightly different from, but still in general agreement with, those of Fig. 4 due to the different system size. The corresponding figure for the NN-model was already given in [12].

Figure 7 shows w_{10} for the HTC model, $N = 256$ and both interaction values $U = 0.5, 2$ at the boundary $p_{+y} = 0$ as a function of the parameter $\nu = (1 - \cos(p_+/2))/2$ with $p_+ = p_{+x}$. The curve for $U = 0.5$ clearly shows a strong local maximum at $\nu \approx 0.5 \pm 0.1$ ($p_+ \approx \pi \pm \pi/8$) corresponding to green-circle with radius $r_g \approx 0.85\pi$ visible in the phase diagram. For $U = 2$ there are higher but less pronounced local maxima at $\nu \approx 0.5 \pm 0.19$ corresponding to the slightly visible circle for this case. However, at $U = 2$ the value of w_{10} at $\nu = 0.5$ is rather high while at $U = 0.5$ its value at $\nu = 0.5$ is quite low but still clearly above the ergodic limit.

Figures S1 and S2 of the supplementary material are similar to Figs. 6 and 7 respectively but for the inverse participation ratio ξ_{IPR} .

We note that of course in the limit of strong interaction between electrons being significantly larger than the energy band width of noninteracting particles ($U \gg 8$) there appear coupled states of pairs forming a separated energy band. However, our theory and numerical results show that the pair formation takes place even at much smaller interactions (e.g. $U = 0.5 \ll 8$). This is the result of an effective narrow energy band appearing due to pair momentum conservation.

6 Time evolution of pair formation

We also computed a more precise time evolution of the pair formation probability w_{10} for the larger system size $N = 384$ and certain specific cases $p_{+x} = p_{+y}$

⁴⁶⁴ ($p_{+x,y} = 0$) or $\nu = 1$ ($p_{+x,y} = 2\pi$) but still clearly
⁴⁶⁵ above the ergodic limit for all cases. The precise numer-

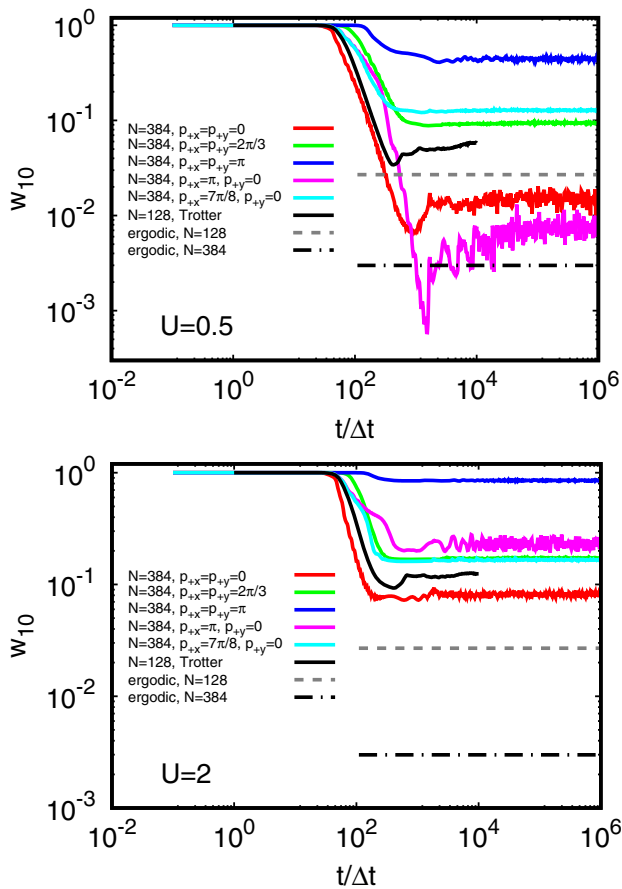


Fig. 8 Time dependence of the pair formation probability w_{10} for $U = 0.5$ (top panel) and $U = 2$ (bottom panel) and different cases of the exact time evolution in certain $\mathbf{p}_+ = (p_{+x}, p_{+y})$ sectors at $N = 384$ and the full space Trotter formula time evolution at $N = 128$. The dashed lines correspond to the ergodic values $(21/N)^2 = 0.0269$ for $N = 128$ (grey dashed) and $(21/N)^2 = 0.00299$ for $N = 384$ (black dashed)

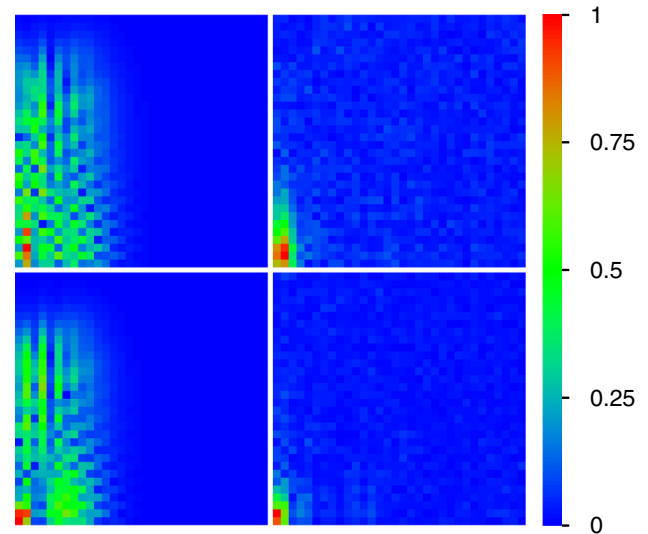


Fig. 9 Color plot of wavefunction amplitude $|\bar{\psi}(\mathbf{p}_+, \Delta \mathbf{r})|$ in block representation in $\Delta \mathbf{r} = (\Delta x, \Delta y)$ plane obtained from the 2D quantum time evolution for the HTC lattice with $N = 384$ and the sector $p_{+x} = 7\pi/8, p_{+y} = 0$. All panels show a zoomed region $0 \leq \Delta x, \Delta y < 32$. Left (right) panels correspond to $t = 100 \Delta t$ ($t = 10^5 \Delta t$; with $\Delta t = 1/B_2 = 1/(16 + U)$) and top (bottom) panels correspond to interaction strength $U = 0.5$ ($U = 2$). Related videos are available at [15]

sponds to an average over all possible \mathbf{p}_+ values, is quite low if compared to the case $\mathbf{p}_+ = 0$ but still clearly above the corresponding ergodic value (for its reduced system size). Also for most of the other cases the saturation value is clearly above the ergodic value except for $U = 0.5, p_{+y} = 0$ and $p_{+x} = \pi$ where the curve is a $t \approx 10^3 \Delta t$ even below the ergodic value and saturates later at a value only slightly above the ergodic value.

Motivated by the observation of the green-circle at radius $r_g \approx 0.85\pi$ in the phase diagram for $U = 0.5$, we show in Fig. 9 the wavefunction amplitude at $p_{+x} = 7\pi/8, p_{+y} = 0, N = 384$ and both interaction values $U = 0.5, 2$ and two time values $t/\Delta t = 100, 10^5$. The first observation is that the diffusive spreading in x -direction is strongly suppressed if compared to the y -direction which is expected since p_{+x} is rather close to π while $p_{+y} = 0$.

At $U = 0.5$ the steady-state at $t/\Delta t = 10^5$, despite a smaller value of $w_{10} = 0.0754$ if compared to $w_{10} = 0.1342$ at $U = 2$, has a larger spatial extension of ~ 30 lattice sites compared to ~ 12 lattice sites for $U = 2$. This is in rough qualitative agreement with the values $\xi_{\text{IPR}} = 940$ (for $U = 0.5$) and $\xi_{\text{IPR}} = 268$ (for $U = 2$). However, a large amount of the contribution to the inverse participation ratio comes from the remaining probability of about 87-90% which has uniformly spread over the full lattice thus explaining the difference between ξ_{IPR} and the visible spatial extension in Fig. 9 (for this reason we consider w_{10} to be a more suitable quantity than ξ_{IPR} to describe the pair formation probability).

$\in \{0, 2\pi/3, \pi\}$ and $p_{+y} = 0$ with $p_{+x} \in \{7\pi/8, \pi\}$. The results together with the full space results using the Trotter formula approximation at $N = 128$ are shown in Fig. 8 for $U = 0.5, 2$. In all cases the value of w_{10} starts decaying from its initial value $w_{10} = 1$ at $t/\Delta t > 20-30$ and converges to a long time saturation value for $t/\Delta t > 10^3$ sometimes with some temporal quasi-periodic fluctuations. In most cases the saturation values at $U = 2$ are clearly larger than for $U = 0.5$ except for the case $p_{+y} = 0$ and $p_{+x} = 7\pi/8$ where both saturation values are somewhat comparable. In particular, at $U = 0.5$ the value for $p_{+y} = 0$ and $p_{+x} = 7\pi/8$ is significantly larger than the value for $p_{+y} = 0$ and $p_{+x} = \pi$ while at $U = 2$ it is the inverse. This observation is in agreement with the appearance of the green-circle in the phase diagram where for $U = 0.5$ the circle is dominant in comparison to the right boundary while for $U = 2$ it is dominated by the right boundary.

The saturation value of the data obtained by the Trotter formula approximation, which somehow corre-

7 Comparison of two lattice models

Above we studied the properties of Coulomb pairs in the two lattice models: the nearest neighbor tight-binding model (NN-model) and the HTC model with the long-ranged hoppings based on the results reported in [6] (see Eq. (4)). We point that our developed general formalism allows to consider the two interacting electrons on a broad type of lattices with long-ranged hoppings. Here we presented the results only for two lattices of NN- and HTC-models.

The main features of the NN-model have been reported in [12]. This model has a certain somewhat specific property that the width of an effective minimal energy band $\Delta E_{b,\min}(\mathbf{p}_+)$ (see Eq. (7)) becomes zero for a certain momentum. However, for the HTC-model the minimal width $\Delta E_{b,\min}(\mathbf{p}_+)$ remains small but finite. In spite of this difference between the two models the formation of Coulomb pairs exists in both models for moderate interactions as it is shown by the results presented above. Another difference between two models is that the kinetic energy E_c (see Eq. (6)) at $\mathbf{p}_1 = \mathbf{p}_2 = \mathbf{p}_+/2$ is zero only at one point in the momentum plane for the NN-model and it is zero along a finite line segment for the HTC-model (see Fig. 1).

In presence of interaction the above differences between two models lead to a very different structure of probability of Coulomb pair formation in the phase diagram in the plane of pair momentum as it is shown in Fig. 4: there is only one maximum of this probability for the NN-model in one point of the plane, while for the HTC-model there is an additional maximum of probability along a “green-circle” in the momentum plane. Thus the phase volume with a significant probability of pair formation is significantly larger for the HTC-model. This feature can play a significant role at finite electron densities where the high space volume is important for specific doping values corresponding to energies of this “green-circle”. Indeed, the results of Fig. 10 show that the range of high pair formation probability, in dependence of doping ν_{2D} , is broader for the HTC-model.

Finally, we point out that the phase diagram of the Coulomb pair formation of Fig. 4 is obtained for both models only in this work (in [12] for the NN-model this probability was obtained only along a line $p_{+x} = p_{+y}$ and not in the whole momentum plane).

8 Results overview

The discussion of the phase diagram given in Fig. 4 has shown that the pair formation probability is maximal at the point $\mathbf{p}_+ = (\pi, \pi)$. However, the surrounding region to this point is quite small if compared to the green-circle where we have a somewhat more modest pair formation probability. In terms of available values of \mathbf{p}_+ the latter region is possibly more important. In order to analyze this point in a more quantitative way,

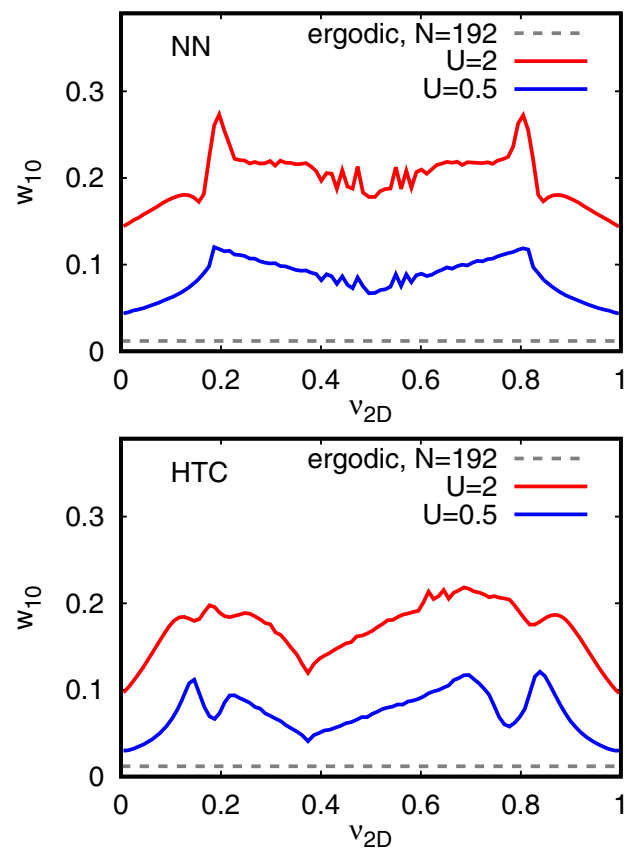


Fig. 10 Dependence of the electron pair formation probability w_{10} on the effective 2D filling factor ν_{2D} for the NN-lattice (top) and the HTC-lattice (bottom). The values of w_{10} have been obtained from the data of Fig. 4 (for $N = 192$) by an average along lines of constant electron pair energy E_c at momenta $\mathbf{p}_1 = \mathbf{p}_2 = \mathbf{p}_+/2$ with $p_{+x}, p_{+y} \in [0, 2\pi]$. Lowest (largest) energy corresponds to $\nu_{2D} = 0$ ($\nu_{2D} = 1$). The data points shown correspond to an effective histogram with bin width $\Delta\nu_{2D} \approx 0.01$. The red (blue) curve corresponds to the interaction value $U = 2$ ($U = 0.5$) and the grey dashed line corresponds to the ergodic value $(21/192)^2 = 0.01196$

we assume a simple model where both electrons have the same momentum $\mathbf{p}_+/2$ (i.e. $\Delta p = 0$) and where the available states of this type are filled from smallest to largest energies. We subdivide these states, ordered in energy, in slices of equal number ($\sim 1/100$ of all available states) and compute the average of w_{10} for each slice which is equivalent to the average of w_{10} at lines of constant energy. In Fig. 10, we show the dependence of this average on the effective 2D-filling factor ν_{2D} which is the weight of slices below a certain energy.

For the NN-model we observe a strong peak at $\nu_{2D} = 0.2$ (and similarly at $\nu_{2D} = 0.8$ due to symmetry). This peak is caused by the combination of the maximum point at $\mathbf{p}_+ = (\pi, \pi)$ and rather strong (top or right) boundary contributions visible in the left panels of Fig. 4. For the HTC-model at $U = 2$ this peak is still visible but its value is reduced. However, for $U = 0.5$, there are two separated peaks, a stronger one

624 at $\nu_{2D} \approx 0.15$ related to the average over the green circle at radius $r_g \approx 0.85$ and a second lower peak at
 625 circle at radius $r_g \approx 0.85$ and a second lower peak at
 626 $\nu_{2D} \approx 0.24$ related to the average of the maximum region close to $\mathbf{p}_+ = (\pi, \pi)$. For this particular case,
 627 the green circle has a stronger global contribution to the pair formation probability than the maximum region at
 628 $\mathbf{p}_+ = (\pi, \pi)$.
 629

630 We note that the size of pairs δr_{2e} is rather small being given by only a few lattice sizes (e.g. $\delta r_{2e} \approx 3$ at
 631 $U = 0.5$ according to Fig. 9). Thus the effective coupling energy of a pair can be estimated as $E_{2e} \approx U/\delta r_{2e}$.
 632 Thus we suppose that for temperatures being smaller than this effective energy gap ($T < E_{2e}$) the thermal
 633 fluctuations, decoherence and dissipative effects will be significantly suppressed. However, the analysis
 634 of decoherence effects should be investigated in further detailed studies.
 635
 636
 637
 638
 639
 640

641 9 Discussion

642 In our studies we analyzed the electron pair formation in a tight-binding model of La-based cuprate superconductors
 643 induced by Coulomb repulsion. Our analytical and numerical results show that even a repulsive
 644 Coulomb interaction can form two electron pairs with a high probability. Such pairs have a compact size and
 645 propagate through the whole system. We expect that such pairs may contribute to the emergence of superconductivity
 646 in La-based cuprates.
 647

648 Of course, our analysis only considers two electrons and in a real system at finite electron density there is a Fermi sea
 649 which can modify electron interactions. However, we expect that electrons significantly below the Fermi energy will
 650 only create a mean-field potential which will not significantly affect interacting electrons with energies in the vicinity
 651 of the Fermi energy. A detailed investigation of effects of finite electron density on the Coulomb pair formation
 652 represents an important task for future studies.
 653

654 In this work we did not solve the problem of La-based cuprate superconductors. Indeed, this is a very complex
 655 problem which remains unsolved since 1986 till present. Here we discuss a new mechanism of formation of
 656 electron pairs by the Coulomb repulsion. We show that our mechanism is rather generic and it works for
 657 repulsive electrons on various types of long-ranged or nearest neighbor hopping lattices. The effects of finite
 658 electron density still should be investigated for this new mechanism. But we hope that the two repulsive
 659 particles approach described here will allow to understand deeper the physics of La-based cuprate superconductors.
 660 Indeed, the size of pairs in cuprates is rather small (about 15 angstroms [2] being only by a factor 10
 661 larger than the inter-atomic distance) compared to the BCS case (with a typical size of about 1000 angstroms
 662 and more [2]). For the Coulomb pairs studied here the pair size is only by a factor 10 larger than the lattice
 663 constant (see e.g. Fig. 3). Thus we expect that future investigations of properties of Coulomb electron pairs
 664
 665
 666
 667
 668
 669
 670
 671
 672
 673
 674
 675
 676
 677
 678
 679
 680

681 at finite density will bring new insights in cuprate type superconductivity. Finally, the Cooper pairs were also
 682 first studied only for two electrons [16].
 683

684 **Acknowledgements** This work has been partially supported through the grant NANOX N° ANR-17-EURE-
 685 0009 in the framework of the Programme Investissements d’Avenir (project MTDINA). This work was granted access
 686 to the HPC resources of CALMIP (Toulouse) under the allocation 2020-P0110.
 687
 688
 689

690 **Data Availability Statement** This manuscript has data included as electronic supplementary material. The online
 691 version of this article contains supplementary material, which is available to authorized users.
 692
 693

694 A Appendix

695 In this appendix we present the derivation of the block Hamiltonian (11) and a more detailed discussion about its
 696 discrete symmetries. In order to simplify the notations, we will use here the full set $\mathcal{A}' = \mathcal{A} \cup (-\mathcal{A})$ of neighbor vectors
 697 (in the full and not only half plane) for the summation over the vectors \mathbf{a} which allows to reduce the number of terms
 698 in the following expressions. The TIP Hamiltonian (5) can then be written in a more explicit form as:
 699
 700
 701
 702

$$\begin{aligned}
 H = & - \sum_{\mathbf{r}_1, \mathbf{r}_2} \sum_{\mathbf{a} \in \mathcal{A}'} t_{\mathbf{a}} (|\mathbf{r}_1, \mathbf{r}_2\rangle \langle \mathbf{r}_1 + \mathbf{a}, \mathbf{r}_2| + |\mathbf{r}_1, \mathbf{r}_2\rangle \langle \mathbf{r}_1, \mathbf{r}_2 - \mathbf{a}|) \\
 & + \sum_{\mathbf{r}_1, \mathbf{r}_2} \bar{U}(\mathbf{r}_2 - \mathbf{r}_1) |\mathbf{r}_1, \mathbf{r}_2\rangle \langle \mathbf{r}_1, \mathbf{r}_2|
 \end{aligned}
 \tag{13}$$

705 where for convenience we have written “ $\mathbf{r}_2 - \mathbf{a}$ ” instead of “ $\mathbf{r}_2 + \mathbf{a}$ ” (in the second term of the first line) since for $\mathbf{a} \in \mathcal{A}'$
 706 also $-\mathbf{a} \in \mathcal{A}'$. Furthermore, the terms with shifts of \mathbf{a} in the left side have been absorbed by the increased set \mathcal{A}' (with
 707 respect to \mathcal{A} used in (1)) combined with a subsequent shift of the summation index \mathbf{r}_1 or \mathbf{r}_2 and exploiting the periodic
 708 boundary conditions.
 709

710 Applying (13) to a block basis state (10) we find that:
 711
 712

$$\begin{aligned}
 H|\mathbf{p}_+, \Delta\mathbf{r}\rangle = & -\frac{1}{N} \sum_{\mathbf{r}_1} \sum_{\mathbf{a} \in \mathcal{A}'} t_{\mathbf{a}} \left(|\mathbf{r}_1 - \mathbf{a}, \mathbf{r}_1 + \Delta\mathbf{r}\rangle \right. \\
 & \times e^{i\mathbf{p}_+ \cdot (\mathbf{r}_1 + \Delta\mathbf{r}/2)} \\
 & \left. + |\mathbf{r}_1, \mathbf{r}_1 + \Delta\mathbf{r} + \mathbf{a}\rangle e^{i\mathbf{p}_+ \cdot (\mathbf{r}_1 + \Delta\mathbf{r}/2)} \right) \\
 & + \bar{U}(\Delta\mathbf{r})|\mathbf{p}_+, \Delta\mathbf{r}\rangle.
 \end{aligned}
 \tag{14}$$

713 Using the shift $\mathbf{r}_1 \rightarrow \mathbf{r}_1 + \mathbf{a}$ in the \mathbf{r}_1 -sum of the first line of this expression we obtain:
 714
 715
 716
 717
 718

$$\begin{aligned}
H|\mathbf{p}_+, \Delta\mathbf{r}\rangle &= -\frac{1}{N} \sum_{\mathbf{r}_1} \sum_{\mathbf{a} \in \mathcal{A}'} t_{\mathbf{a}} \left(|\mathbf{r}_1, \mathbf{r}_1 + \Delta\mathbf{r} + \mathbf{a}\rangle \right. \\
&\quad \times e^{i\mathbf{p}_+ \cdot (\mathbf{r}_1 + \mathbf{a} + \Delta\mathbf{r}/2)} \\
&\quad \left. + |\mathbf{r}_1, \mathbf{r}_1 + \Delta\mathbf{r} + \mathbf{a}\rangle e^{i\mathbf{p}_+ \cdot (\mathbf{r}_1 + \Delta\mathbf{r}/2)} \right) \\
&\quad + \bar{U}(\Delta\mathbf{r})|\mathbf{p}_+, \Delta\mathbf{r}\rangle \quad (15)
\end{aligned}$$

which can be rewritten as:

$$\begin{aligned}
H|\mathbf{p}_+, \Delta\mathbf{r}\rangle &= -\frac{1}{N} \sum_{\mathbf{r}_1} \sum_{\mathbf{a} \in \mathcal{A}'} t_{\mathbf{a}} |\mathbf{r}_1, \mathbf{r}_1 + \Delta\mathbf{r} + \mathbf{a}\rangle \\
&\quad \times e^{i\mathbf{p}_+ \cdot [\mathbf{r}_1 + (\Delta\mathbf{r} + \mathbf{a})/2]} \underbrace{\left(e^{i\mathbf{p}_+ \cdot \mathbf{a}/2} + e^{-i\mathbf{p}_+ \cdot \mathbf{a}/2} \right)}_{2 \cos(\mathbf{p}_+ \cdot \mathbf{a}/2)} \\
&\quad + \bar{U}(\Delta\mathbf{r})|\mathbf{p}_+, \Delta\mathbf{r}\rangle \\
&= -2 \sum_{\mathbf{a} \in \mathcal{A}'} t_{\mathbf{a}} \cos(\mathbf{p}_+ \cdot \mathbf{a}/2) |\mathbf{p}_+, \Delta\mathbf{r} + \mathbf{a}\rangle \\
&\quad + \bar{U}(\Delta\mathbf{r})|\mathbf{p}_+, \Delta\mathbf{r}\rangle. \quad (16)
\end{aligned}$$

The last expression provides exactly the effective block Hamiltonian (11) if we replace the sum over $\mathbf{a} \in \mathcal{A}'$ by a sum over $\mathbf{a} \in \mathcal{A}$ with two contributions “+ \mathbf{a} ” and “- \mathbf{a} ” and applying for the latter contribution a subsequent shift $\Delta\mathbf{r} \rightarrow \Delta\mathbf{r} + \mathbf{a}$ in the $\Delta\mathbf{r}$ sum. However, there is one additional complication if $\Delta\mathbf{r} + \mathbf{a} = (\Delta x + a_x, \Delta y + a_y)$ in (16) leaves the initial square of $\Delta x, \Delta y \in \{0, \dots, N-1\}$. Then we have to add (subtract) N to (from) $\Delta x + a_x$ and/or $\Delta y + a_y$ which provides according to (10) the factor $e^{\pm i p_{+x} N/2} = e^{\pm i \pi l_{+x}} = (-1)^{l_{+x}}$ (for Δx and similarly for Δy) resulting in either periodic or anti-periodic boundary conditions in x - (y -)direction depending on the parity of the integer index l_{+x} (l_{+y}).

We close this appendix with a short discussion about the discrete reflection symmetries of the block Hamiltonian (11) and the possibility to reduce its effective matrix size N^2 due to such symmetries. For the NN-model, as already discussed in detail in [12], there are at least two symmetries with respect to $\Delta x \rightarrow N - \Delta x$ (reflection at the Δy -axis) or $\Delta y \rightarrow N - \Delta y$ (reflection at the Δx -axis) and in case if $p_{+x} = p_{+y}$ there is a third symmetry with respect to $\Delta x \leftrightarrow \Delta y$ (reflection at the Δx - Δy diagonal) which allows for an effective matrix size of roughly either $N^2/4$ or $N^2/8$ (if $p_{+x} = p_{+y}$).

However, for a more general lattice, such as the HTC-model, or more generally in presence of at least one neighbor vector $\mathbf{a} = (a_x, a_y)$ with both $a_x \neq 0$ and $a_y \neq 0$ (e.g. $\mathbf{a} = (1, 1)$) the number of symmetries is reduced. For the most generic case with $p_{+x} \neq p_{+y}$, $p_{+x} \neq 0$ and $p_{+y} \neq 0$ there is only one symmetry corresponding to particle exchange with two simultaneous transformations $\Delta x \rightarrow N - \Delta x$ and $\Delta y \rightarrow N - \Delta y$ which allows for a reduction of the effective matrix size to $\approx N^2/2$. In this case the factors $\cos(\mathbf{p}_+ \cdot \mathbf{a}/2) = \cos[(p_{+x} a_x + p_{+y} a_y)/2]$ appearing in

the effective hopping amplitudes are not modified because the replacement $\mathbf{a} \rightarrow -\mathbf{a}$ due the symmetry transformation only changes the global sign inside the cosine argument. However, this is no longer true if we apply for example the transformation $\Delta x \rightarrow N - \Delta x$ without modifying Δy which is equivalent to the replacement of $(a_x, a_y) \rightarrow (-a_x, a_y)$ of the neighbor vectors. Therefore a **single** reflection at the Δy (or Δx) axis modifies the hopping amplitude (if both $a_x \neq 0$, $a_y \neq 0$ and also both $p_{+x} \neq 0$, $p_{+y} \neq 0$) and (11) is (in general) not invariant with respect to such transformations. However, if either $p_{+x} = 0$ or $p_{+y} = 0$ the effective hopping amplitudes are not modified with respect to these two individual reflections and we have two symmetries with an effective matrix size of $\approx N^2/4$. Also if $p_{+x} = p_{+y} \neq 0$ we have two symmetries (particle exchange and reflection at the Δx - Δy diagonal) leading also to an effective matrix size of $\approx N^2/4$. Finally, for the special case $p_{+x} = p_{+y} = 0$, we have even three symmetries (as in the NN-Model for $p_{+x} = p_{+y}$) with effective matrix size of $\approx N^2/8$.

References

1. K.A. Müller, J.G. Bednorz, Z. Phys. B Condens. Matter **64**, 189 (1986)
2. E. Dagotto, Rev. Mod. Phys. **66**, 763 (1994)
3. B. Keimer, S.A. Kivelson, M.R. Norman, S. Uchida, Z. Zaanen, Nature **518**, 179 (2015)
4. C. Proust, L. Taillefer, Annu. Rev. Condens. Matter Phys. **10**, 409 (2019)
5. P.W. Anderson, Science **235**, 1196 (1987)
6. R. Photopoulos, R. Fresard, Ann. Phys. (Berlin) **2019**, 19001771900177 (2019)
7. V.J. Emery, Phys. Rev. Lett. **58**, 2794 (1987)
8. V.J. Emery, G. Reiter, Phys. Rev. B **38**, 4547 (1988)
9. C.M. Varma, Solid State Commun. **62**, 681 (1987)
10. Y.B. Gaididei, V.M. Loktev, Phys. Status Solidi **147**, 307 (1988)
11. R.S. Markiewicz, S. Sahrakorpi, M. Lindroos, H. Lin, A. Bansil, Phys. Rev. B **72**, 054519 (2005)
12. K.M. Frahm, D.L. Shepelyansky, Phys. Rev. Research **2**, 023354 (2020)
13. K.M. Frahm, D.L. Shepelyansky, Eur. Phys. J. B **89**, 8 (2016)
14. See Supplemental Material at <http://XXXX> that contains extra-figures and videos supporting the main conclusions and results
15. K.M. Frahm, D.L. Shepelyansky, Available upon request: <https://www.quantware.ups-tlse.fr/QWLIB/electronpairsforhtc/>. Accessed Sep. (2020)
16. L. Cooper, Phys. Rev. **104**, 1189 (1956)